IMPERIAL COLLEGE LONDON
DEPARTMENT OF PHYSICS

SPC-Czaja-1

Sea Surface Temperature Anomalies and the Slab Mixed Layer Model: A Review

Chengyun Zhu

Supervisor: Arnaud Czaja

Assessor: Paulo Ceppi

[2497 words]

October 5, 2025

Submitted in part fulfilment of the requirements for the degree of Master in Science in Physics of Imperial College London and the Diploma of Imperial College London.

Declaration of Originality

I, Chengyun Zhu, declare that the work in this review is my own. The work of others has been appropriately referenced. A full list of references is given in the bibliography.

Abstract

Sea Surface Temperature Anomalies (SSTA) are crucial to the study of climate dynamics. Their evolution depends on air-sea processes, ocean advection, and vertical mixing within the upper ocean. This review first provides an overview of the structure and changes in global sea surface temperature, then evaluates upper ocean models of major categories such as KPP, PWP, and GLS, and introduces a slab mixed layer model by Czaja [1] - a simplified but physically based framework for studying SSTA dynamics. The applicability of datasets including ARGO, ERA5, and satellite altimetry is considered in model evaluation and parameter estimation. This review discusses the advantages and limitations of the slab mixed layer model, particularly its practicality in exploring the persistence, variability, and feedback aspects of SSTA within computationally tractable frameworks.

Acknowledgements

When I was a child, I was deeply fascinated by Earth science: from the atmosphere to the ocean, from planets to animals, from water vapour to clouds; I loved exploring all of these topics in encyclopaedias.

When I enrolled in the Department of Physics at Imperial College—a privilege for which I feel very fortunate—I was thrilled, convinced that my passion would guide my path. I am especially grateful to Professor Helen Brindley, my personal tutor and the lecturer in Environmental Physics, whose teaching was rich with insight; and to Dr Edward Gryspeerdt and Dr Paulo Ceppi, whose teaching in Atmospheric Physics during my third year was both engaging and inspiring.

I would also like to thank my supervisor, Dr Arnaud Czaja, for giving me this invaluable opportunity to dive into climate science. I am really looking forward to any feedback from you at any stage.

And to all my friends.

Finally, I have done my best to write this literature review in a way that is easy to understand; even to my parents, who have always supported me with unwavering encouragement. Their emotional support and financial sacrifices have allowed me to pursue higher education, for which I am deeply grateful.

I acknowledge the use of generative AI, chatGPT by openAI, for proofreading this literature review. Any new information had been carefully cross-checked and evaluated.

Dedication

Kal’tsit’s dimensions in life cannot be measured.

Amid countless possible identities, she steadfastly holds to her own choices.

Those who walk alongside her are also painting their own stories.

Time never stands still, and Kal’tsit moves forward with it.

"We cannot escape the past, but the future ahead of you will be different. "

Kal’tsit

"Even if the ocean boils away and the atmosphere vanishes,

Even if all the moons in the sky are pulled into the vortex of our planet’s gravity,

At the far end of our civilisation, I am sure we will meet again.

I promise you I will.

Wait for me, you must wait for me too.

Don’t ever forget about me.

Oracle"

Contents

List of Figures

Chapter 1

Introduction

Sea Surface Temperature (SST) is a linchpin of climate science. The ocean covers approximately 71 percent of the Earth's surface, and its surface temperature is a crucial variable in global climate models and weather forecasts [2, 3, 4]. Research on SST also supports applications in fisheries management, tourism, and assessments of ecological change. The Sea Surface Temperature Anomaly (SSTA) refers to the deviation of observed SST from the long-term climatological mean for a given location and time, typically calculated over several decades (Fig. 1.1). SSTA has been shown to exert a significant influence on atmospheric processes [5] and is a key parameter in studies of climate variability and long-term climate change [2]. An example is the El Niño–Southern Oscillation (ENSO), a well-known climate phenomenon that originates in the tropical Pacific, and has serious impacts on global weather extremes [6, 7]. Beyond the tropics, SSTA in mid-latitudes can influence the recurrence of severe winters [8], the modulation of marine heatwaves [9], and the development of extratropical cyclones [10, 11]. These broad impacts make understanding and predicting SSTA a key priority in climate science.

However, it is still challenging to model SSTA precisely. Even the most advanced coupled climate models are subject to SST biases, such as warm biases at the eastern and western boundary of the tropical Pacific, and cold biases in the North Atlantic [12, 13]; these biases are also visible in Fig. 1.1. These errors will propagate due to circulation and limit the ability of seasonal to decadal forecasting. In addition, the pattern of SST changes itself also plays an important feedback role: recent studies have shown that the spatial distribution of SST changes has slowed the pace of global warming via "pattern effects" [14].

To address this challenge, various methods have been developed. Coupled General Circulation Models (CGCMs), while capable of providing comprehensive simulations, are computationally expensive and prone to sea surface temperature biases [12]. Empirical and hybrid frameworks, such as analogue prediction, have been used to predict seasonal SSTA and have achieved varying degrees of success [15]. More models for the upper ocean are introduced in Chapter 3. Recently, machine learning and hybrid physics-data methods have emerged, providing effective tools for prediction, but also raising concerns about interpretability and robustness [16, 17].

This review places the slab mixed layer model within a broader scope of understanding and predicting SSTA. It outlines the motivations for SST modelling, challenges in limiting predictability, and the scope of existing models, and then considers the opportunities and limitations of this model as an interactive climate analysis tool.

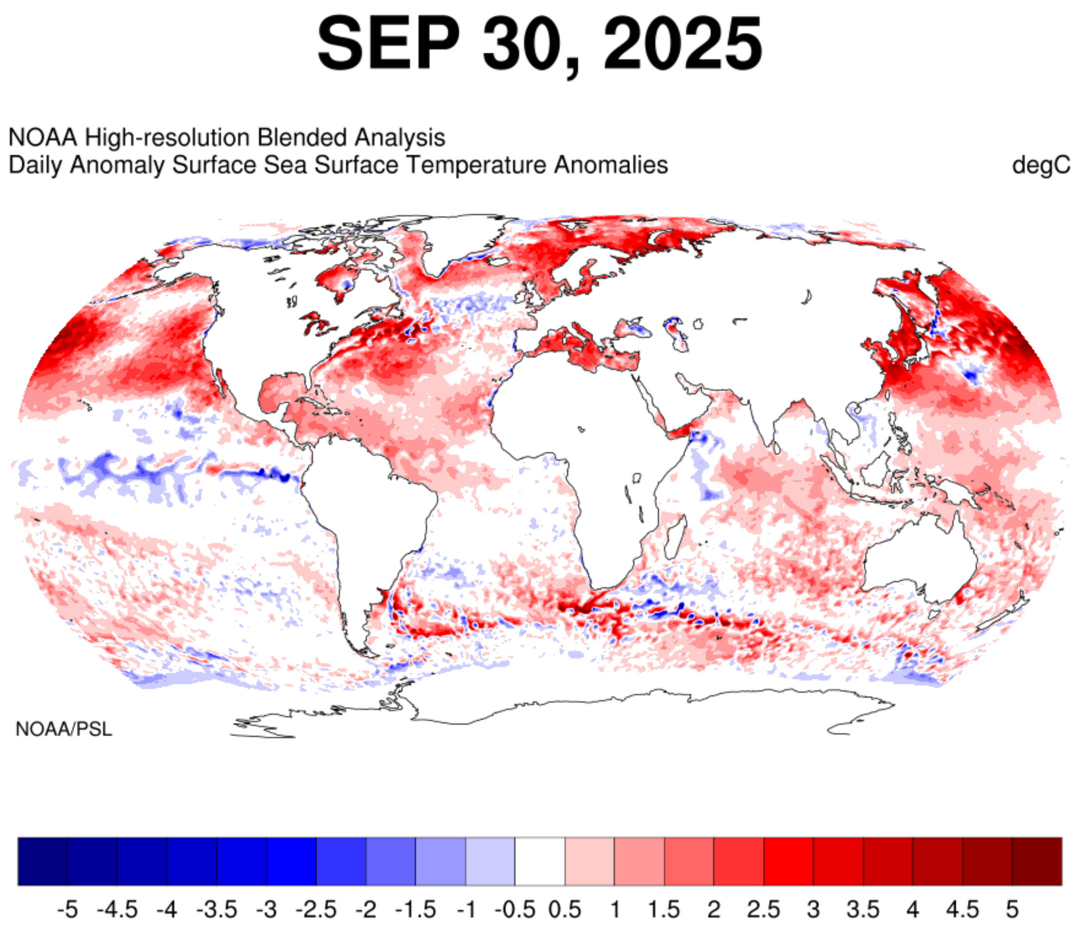

Figure 1.1: Sea Surface Temperature Anomalies on 30 September 2025, computed as observed daily SST minus the 1991–2020 climatological mean.
Data source: NOAA OI SST V2 High Resolution Dataset, provided by the NOAA PSL, Boulder, Colorado, USA, from their website at https://psl.noaa.gov [18].

Chapter 2

Overview of SST and SSTA

This chapter reviews the basic temperature structure of the ocean. Observational studies have shown that the persistence of SSTA is highly dependent on the Mixed Layer Depth (MLD) and vertical processes such as entrainment[1] and restratification[2], highlighting the importance of accurately representing upper ocean dynamics [2, 19, 20].

2.1 Vertical Temperature Profile of the Ocean

During the past century, researchers have described the vertical temperature profile of the ocean, which is conventionally divided into three zones [21]. The upper mixed layer, which typically extends from the surface to depths of $50-200\,m$, maintains temperatures comparable to those at the surface. Beneath this lies the thermocline, where temperature decreases sharply with depth. Below the thermocline is a deep layer zone, characterised by a relatively stable thermal profile. Regional variations are also observed; for example, at high latitudes a dicothermal layer may form, consisting of water that is colder than both the overlying mixed layer and the underlying thermocline. SST in temperate zones is highly dependent on seasonal cycles.

The typical temperature-depth profiles of the ocean are shown in Fig. 2.1.[3] Note that these figures are from three specific floats, instead of averaged results. This is because of the substantial size of the ARGO data files. This vertical stratification strongly affects the persistence and evolution of SSTA.

[1] Entrainment refers to turbulent mixing, which draws colder thermocline water into the mixing layer.

[2] Restratification is the process of making the mixing layer shallower under stable surface heating.

[3] These data were collected and made freely available by the International ARGO Programme and the national programmes that contribute to it. (`https://argo.ucsd.edu`, `https://www.ocean-ops.org`). The ARGO Programme is part of the Global Ocean Observing System.

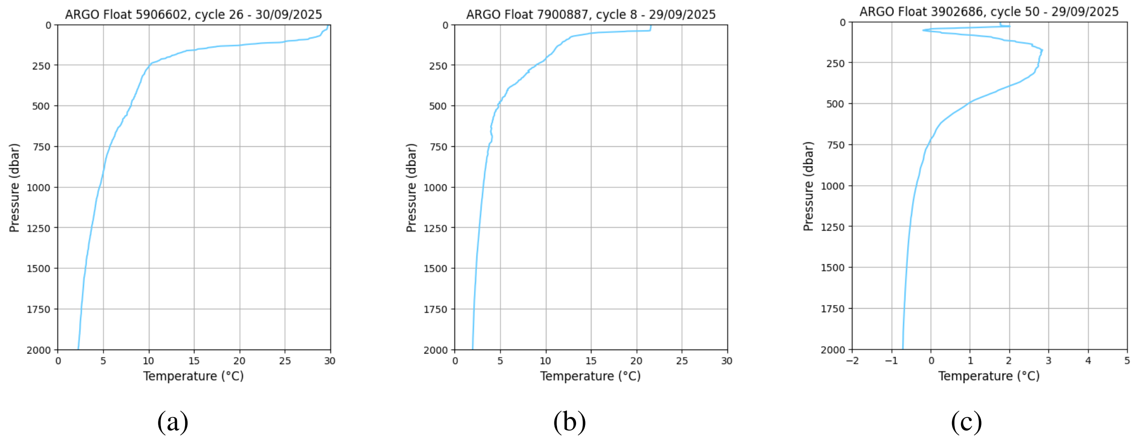

Figure 2.1: Typical temperature-depth profiles of the ocean in (a) tropical, (b) temperate, and (c) frigid. Unit *dbar* is frequently used in oceanography, and 1 *dbar* approximately equals 1 *m* of seawater depth.
Data source: ARGO [22, 23]. Further details are provided in Chapter 4.

2.2 SST and SSTA: Global Profile

In open waters, SST exhibits an approximate zonal distribution, with isotherms typically arranged in an east-west direction. This is due to the heat budget received at the surface; tropical regions receive much more energy from the Sun than polar regions due to astronomical geometry. Therefore, mean SST is highest near the equator and decreases towards the poles, typically showing sharp gradients in mid-latitude regions [21]. This zonal symmetry is altered by circulation characteristics: strong polar transport in western boundary currents such as the Gulf Stream and the Kuroshio Current creates a strong meridional contrast, while coastal upwelling along the eastern boundary introduces local cold zones [21, 24]. Notably, SST exhibits a long-term warming trend of approximately $0.1\,K$ per decade [19, 25], consistent with other estimates cited within the Intergovernmental Panel on Climate Change (IPCC) Assessment Review 6 [26]. It is also worth mentioning the "global warming hiatus" in the early 2000s. This reduction might be attributed to volcanic and solar activity, and internal decadal changes [27].

Fig. 2.2 shows the variability of SSTA on different time scales. Long-term local trends are removed to separate "residual anomalies". Bulgin, Merchant, and Ferreira [19] showed that while the global average signal is mainly dominated by anthropogenic forcing, the evolution of regional SSTA is shaped by dynamic processes such as Kelvin waves and Tropical Instability Waves, both of which are coupled with ENSO. ENSO generates anomalies exceeding $\pm 2\,K$ and drives remote correlations affecting the global climate system [6, 7]. A few regions are of particular interest in studying SSTA, i.e. the Atlantic Meridional Variability region, where exhibits Atlantic Multidecadal Oscillation [28, 29]. In the North-East Pacific there exists the Pacific Decadal Oscillation, causing significant impacts on fisheries [30, 31].

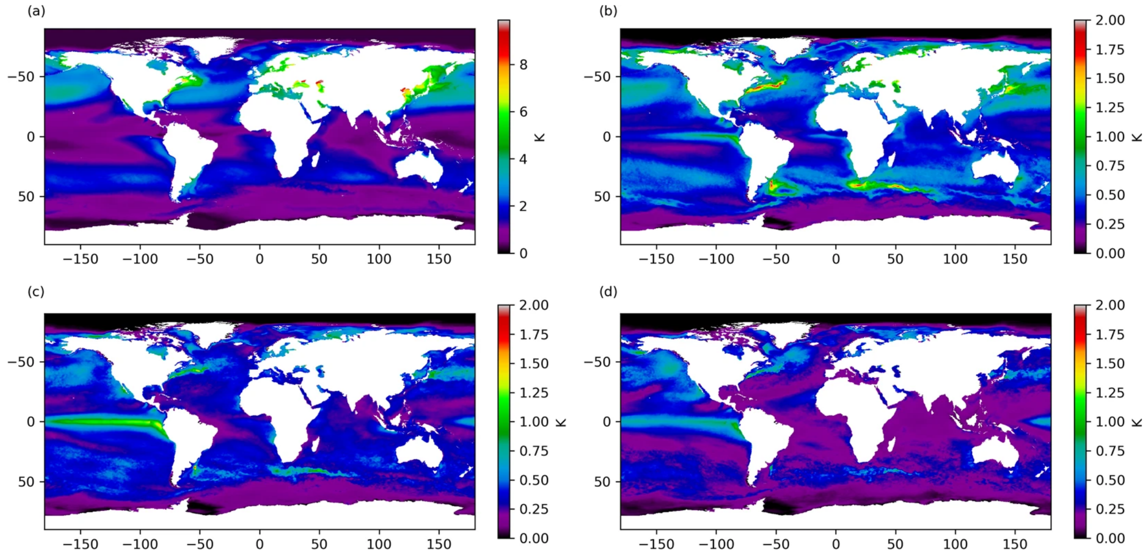

Figure 2.2: (a) SST variability in the monthly climatology from 1982–2010. (b–d) SST integrated amplitude attributable to different parts of the SST power spectrum: (b) sub-annual timescales, (c) timescales of 1–5 years, (d) timescales longer than 5 years. Figure cited from [19].

Chapter 3

Models for the Upper Mixed Layer

The study of SSTA has been explored through various models, ranging from conceptual frameworks to turbulence solutions, from one-dimensional schemes to advection-inclusive approaches, with the slab mixed layer model representing the simplest physics-based choice.

3.1 Early Conceptual and Statistical Model

Hasselmann [32] introduced a Stochastic Climate Model (SCM) in 1976 that considers the oceanic mixing layer as an integrator of stochastic atmospheric forcing. This model can reproduce some observed statistical characteristics of variability [33], and it clearly distinguishes between the characteristics of the weather (short-term response) and the characteristics of the climate (long-term response) [32]. These methods are still valuable for understanding the spectra and persistence, but they lack clear representations of entrainment and restratification.

3.2 Turbulent Kinetic Energy Models

Garwood [34] researched on turbulent kinetic energy closure, tracks production through changes in shear, buoyancy flux, dissipation, and MLD caused by entrainment or restratification. The vertical distributions of eddy diffusivity and viscosity are parameterised as functions of the local turbulent kinetic energy, which is prognostic [35]. Two representative approaches are mentioned here: the Turbulent Kinetic Energy (TKE) model by Gaspar, Grégoris, and Lefevre [36], and the Generic Length Scale (GLS) framework introduced by Burchard et al. [37]. These two models use the same principle for vertical mixing parameterisation [38].

3.3 Other Mixed Layer Models

Large, McWilliams, and Doney [39] introduced "K profile parameterization" (KPP) in 1994, which specifies the vertical diffusivity profile within the mixed layer and adds a non-local transport term to represent the characteristics of the convective plume of the mixed boundary layer. This development marks an important step towards realism, and KPP is now the standard for many climate and ocean circulation models.

The Price-Weller-Pinkel (PWP) model uses convection regulation, which instantly homogenises the unstable vertical profiles generated by solar heating, surface cooling, and air-sea interactions [40]. These mechanisms enable PWP to reproduce the diurnal warming and inertial oscillations of the upper ocean.

In 2019 a research compared five mixed layer surface models using observations in the North Atlantic [38]. Fig. 3.1 shows the performance of five models. In terms of SST, PWP shows the lowest whole year bias, making it a valuable model for simulating SST. GLS has the second-lowest whole year bias; but no model has reproduced the coldest SST observed, and the cold bias in winter. This result is consistent with existing research, and suggests that a global SSTA model is of great importance [12].

3.4 Slab Mixed Layer Model

This section briefly introduces a slab mixed layer model proposed by Czaja [1], and serves as a descriptive theory section for physical processes in the upper ocean.

3.4.1 Slab Mixed Layer Heat Budget Equation

The key idea of the slab mixed layer is to treat its temperature as an averaged value. Mathematically, for a grid cell g characterised by longitude and latitude (x, y) on the Earth's surface, its temperature $\bar{T}$ is:

$$\bar{T}(g,t) = \frac{1}{h(g,t)} \int_{-h(g,t)}^{0} T(x,y,z,t)dz, \tag{3.1}$$

where t is the time and z is the depth. h is the Mixed Layer Depth (MLD), defining the depth where the vertical averaging is physically reasonable. For example, a definition for MLD is the depth at which the water temperature is 1 °C lower than at the sea surface.

[4] The coloured bars at the base of the panels mark the seasons: blue = autumn; green = winter; magenta = spring; cyan = summer. An aside: DJF and JJA are two common abbreviations in climatology, where DJF is the meteorological winter for Dec, Jan, Feb, and JJA is the meteorological summer for Jun, Jul, Aug.

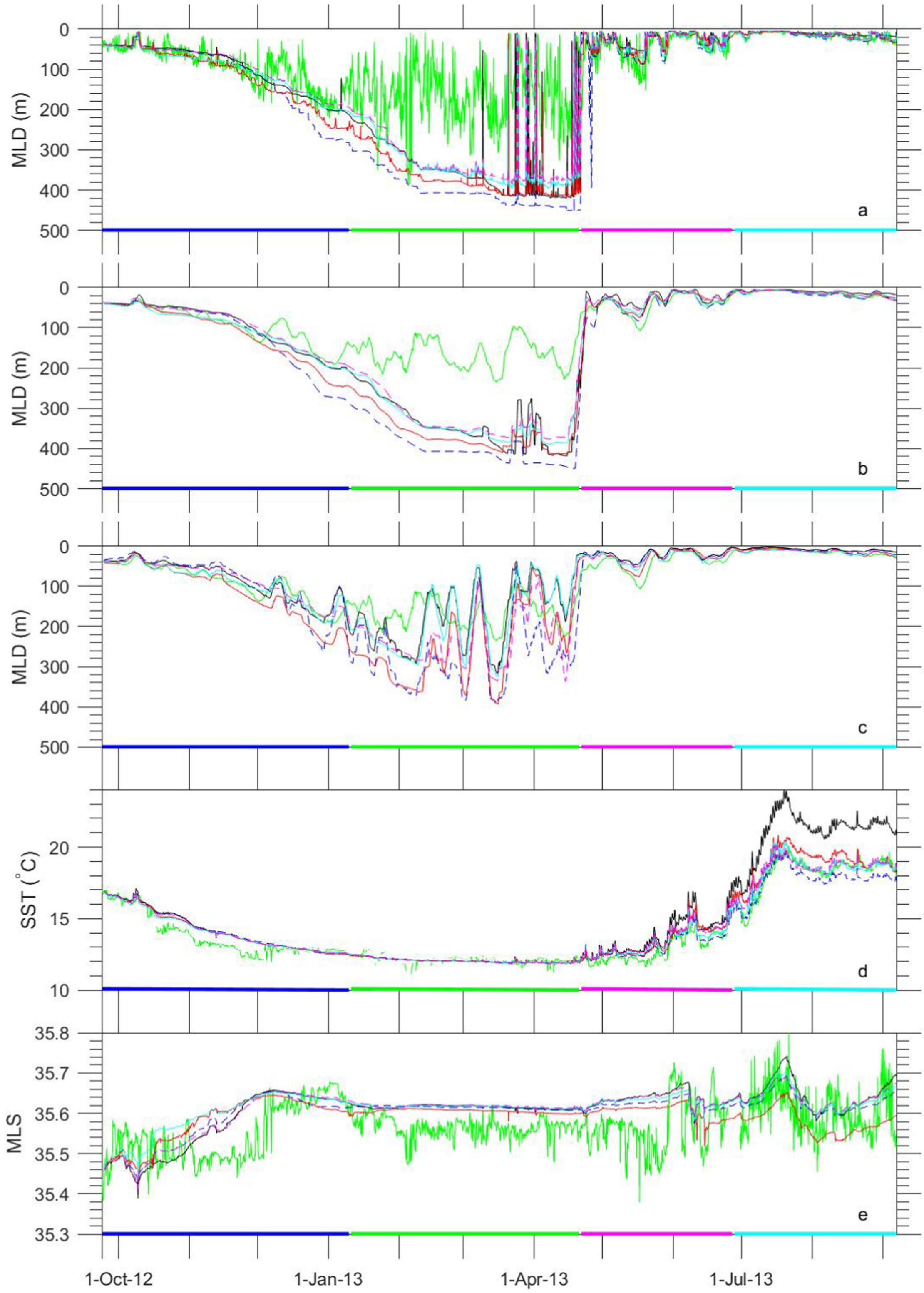

Figure 3.1: The mixed layer and sea surface characteristics from observations and five models over a year in North Atlantic. (a) MLD. (b) MLD smoothed by 5-day averaging. (c) The observed MLD and the internal MLD of the model smoothed. (d) SST. (e) Mixed Layer Salinity. In all panels, green line = observations, dashed blue line = PWP, cyan line = GLS, dashed magenta line = TKE, black line = KPP, red line = OSMOSIS model (not introduced in this review).[4] Figure cited from [38].

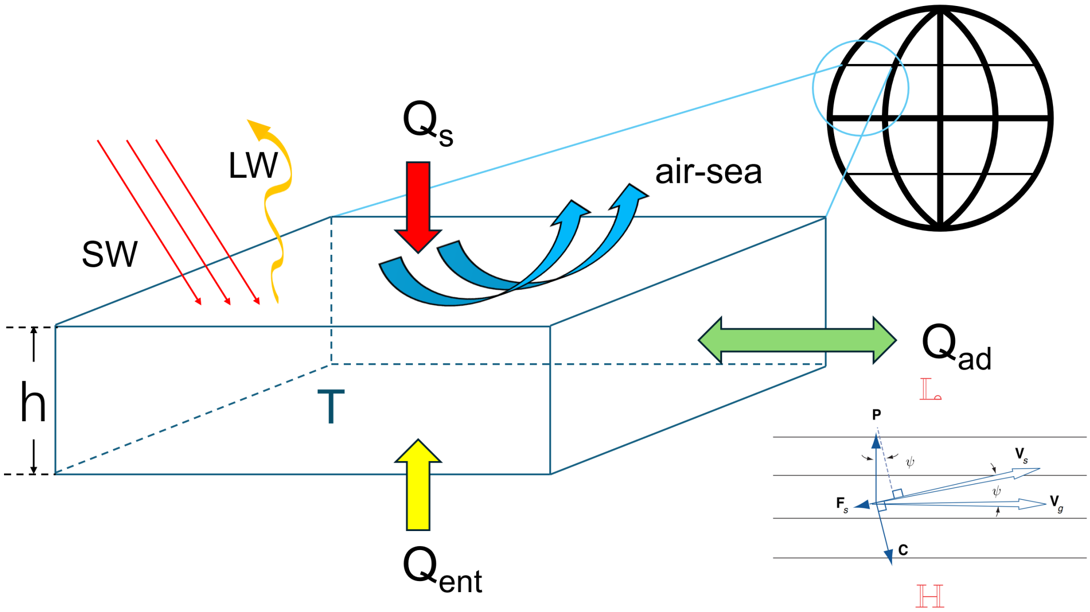

Figure 3.2: Schematic of the slab mixed layer model, proposed by Czaja [1]. The figure on the bottom right is cited from [41].

Fig. 3.2 is a schematic of the slab mixed layer model. In this model, Q_s is the net heat flux at the surface, Q_{ent} is the net heat flux at the bottom of the slab caused by entrainment, and Q_{ad} is the net heat flux exchange with the surrounding due to advection. Since we on on Earth, a rotating frame of reference, it is natural to decompose the advection term into two parts: the geostrophic component Q_{geo}[5] and the Ekman term Q_{Ek}[6].

Now we have all the heat flux terms. The heat budget equation is expressed as:

$$\frac{\partial \bar{T}}{\partial t} = \frac{Q_s + Q_{ent} + Q_{geo} + Q_{Ek}}{c_o \rho_o h}, \tag{3.2}$$

where $c_o \simeq 4100\, J\, kg^{-1}\, K^{-1}$ is the specific heat capacity of seawater, $\rho_o \simeq 1025\, J\, kg\, m^{-3}$ is the typical surface density. Note that all the Q terms are fluxes, in units of $W\ m^{-2}$.

3.4.2 Surface - Radiation and Air-Sea Processes

In Fig. 3.2, Q_s can be mainly decomposed into two parts: radiation Q_{rad} and air-sea processes Q_{a-s}. Radiation consists of inbound solar shortwave radiation, and outbound terrestrial longwave radiation. Q_{a-s} is dependent to speed, temperature and humidity of the air.

[5]Geostrophic current in the direction parallel to isobars (lines of constant pressure). Resulted by the balance of the pressure gradient force and the Coriolis force.

[6]Friction is not negligible close to the surface. The direction of the current is usually determined by a three-way balance, shown on the bottom right of Fig. 3.2.

3.4.3 Entrainment and Restratification

When the mixed layer deepens, cooler water is introduced from the below thermocline, reducing the temperature of the mixing layer. This process can be simplified to:

$$Q_{ent} = c_o \rho_o w_e (T_{sub} - \bar{T}), \tag{3.3}$$

where w_e is the entrainment velocity, and T_{sub} is the temperature of the water below. From Fig. 3.1, entrainment mainly occurs from autumn to winter. Rapid shallowing of MLD (restratification) in spring occurs rapidly, so its impact on SST can be ignored. Thus, w_e can be approximated as:

$$w_e \simeq \begin{cases} \frac{\partial h}{\partial t} & when \frac{\partial h}{\partial t} > 0 \\ 0 & othervise \end{cases}. \tag{3.4}$$

3.4.4 Advection - Geostrophic and Ekman

In this simple model, geostrophic advection is computed from sea surface height $\eta(x,y,t)$. This is the deviation from the geoid. Q_g is given by:

$$Q_g = c_o \rho_o h \frac{g}{f} \left(\frac{\partial \eta}{\partial y} \frac{\partial \bar{T}}{\partial x} - \frac{\partial \eta}{\partial x} \frac{\partial \bar{T}}{\partial y} \right), \tag{3.5}$$

where g is the gravitational acceleration and f is the Coriolis parameter.

Ekman Mass Transport arises from the surface wind stress. Q_{Ek} is given by:

$$Q_{Ek} = c_o \left(\frac{\tau_x}{f} \frac{\partial \bar{T}}{\partial y} - \frac{\tau_y}{f} \frac{\partial \bar{T}}{\partial x} \right), \tag{3.6}$$

where τ_x, τ_y are the components of surface wind stress.

Chapter 4

Datasets

4.1 ARGO Dataset

The ARGO programme (Array for Real-time Geostrophic Oceanography) was conceived in 1999. By the mid-2000s, the array had reached global coverage, and by 2019, more than 2 million temperature salinity profiles had been collected, transforming in-situ ocean monitoring and making significant progress in climate and circulation research [42, 23].

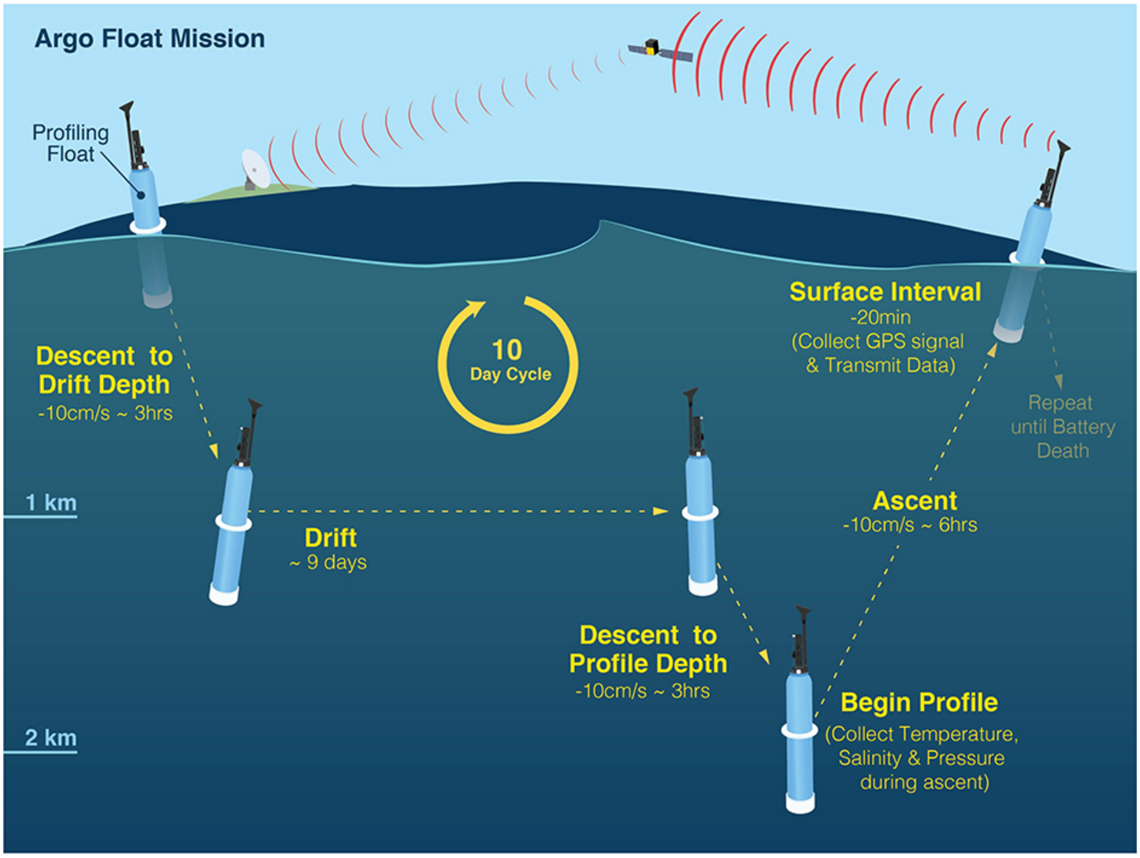

Figure 4.1: Schematic of a standard ARGO float mission. Figure cited from [23].

Fig. 4.1 shows a typical ARGO mission. It measures temperature, salinity and pressure profile of the ocean during ascent. T_{sub} in Eq. (3.3) can be collected from ARGO.

Due to the irregular distribution of ARGO floats in space and time, gridded products have been developed to support large-scale analysis, i.e. the RG-ARGO dataset by Roemmich and Gilson [43]. RG-ARGO is particularly valuable for climate research that requires continuous and spatially complete fields. ARGO data are distributed as thousands of NetCDF files, which contain various variables, metadata, and quality control indicators. Using open-source Python package *argopy*, data can be accessed by region, float number, or configuration file, and returned in an analysis-ready structure, such as the xarray dataset of multidimensional arrays [44].

4.2 ERA5 Dataset

European Centre for Medium-Range Weather Forecasts (ECMWF) Reanalysis v5 (ERA5) is the fifth atmospheric reanalysis produced by the Copernicus Climate Change Service at ECMWF [45]. ERA5 dataset ranges from January 1940 to present, and provides hourly estimates on atmospheric and oceanic parameters. Q_s and Q_{Ek} from Eq. (3.2) can be estimated from this dataset.

ERA5 dataset can be accessed by (a) downloading to a local machine from the Climate Data Store (CDS), (b) installing *cdsapi* package in Python. Both methods require valid CDS account.

4.3 Satellite Altimetry Dataset

Several satellite altimetry datasets are available; only DUACS is introduced here. DUACS stands for Data Unification and Altimeter Combination System, developed by Centre national d'études spatiales (CNES) and Collecte Localisation Satellites (CLS) [46]. DUACS stores a total of 100 years of cumulated data, and can provide the η needed to compute Q_{geo} in Eq. (3.2). Similar to ERA5, DUACS can be accessed by *cdsapi* as well.

Chapter 5

Discussion and Conclusion

The slab mixed layer model is a relatively simple model; this reduces computational difficulty, but it also constrains its capacity to reproduce fine-scale physical variability.

In reality, the interaction between the ocean and the atmosphere is highly dynamic [47]. Surface winds affect turbulent heat flux and ocean mixing, humidity controls latent heat exchange, and cloud layers regulate radiation input. Entrainment is also much more complicated. Turbulent mixing, internal waves, and shear instability can all lead to entrainment on smaller spatial and temporal scales. Models such as PWP, KPP, and GLS attempt to explicitly address these processes through turbulent closure schemes, enabling them to capture i.e. diurnal cycles. Air-sea interactions on a small-scale (mesoscale) can also significantly influence the large-scale climate [48]. Nevertheless, the slab mixed layer model is very suitable as a starting point; the simplified physical processes allow it to be computationally tractable.

In conclusion, SST and SSTA are crucial variables in understanding the global climate. The slab mixed layer model, an anomaly model, is simplified but physically based.

Bibliography

1. Czaja A. Notes on Slab Mixed Layer Heat Budget. [unpublished]. Imperial College London. 2025 Jun
2. Frankignoul C. Sea Surface Temperature Anomalies, Planetary Waves, and Air-sea Feedback in the Middle Latitudes. eng. Reviews of geophysics (1985) 1985; 23:357–90
3. O'Carroll AG, Armstrong EM, Beggs HM, Bouali M, Casey KS, Corlett GK, Dash P, Donlon CJ, Gentemann CL, Høyer JL, Ignatov A, Kabobah K, Kachi M, Kurihara Y, Karagali I, Maturi E, Merchant CJ, Marullo S, Minnett PJ, Pennybacker M, Ramakrishnan B, Ramsankaran R, Santoleri R, Sunder S, Saux Picart S, Vázquez-Cuervo J, and Wimmer W. Observational Needs of Sea Surface Temperature. Frontiers in Marine Science 2019; Volume 6 - 2019. DOI: 10.3389/fmars.2019.00420. Available from: https://www.frontiersin.org/journals/marine-science/articles/10.3389/fmars.2019.00420
4. Mogensen KS, Hewson T, Keeley S, and Magnusson L. Effects of Ocean Coupling on Weather Forecasts. 2018 Jul. Available from: https://www.ecmwf.int/en/newsletter/156/news/effects-ocean-coupling-weather-forecasts
5. Zhou G. Atmospheric Response to Sea Surface Temperature Anomalies in the Mid-latitude Oceans: A Brief Review. Atmosphere-Ocean 2019; 57:319–28. DOI: 10.1080/07055900.2019.1702499. Available from: https://doi.org/10.1080/07055900.2019.1702499
6. McPhaden MJ, Zebiak SE, and Glantz MH. ENSO as an Integrating Concept in Earth Science. Science 2006; 314:1740–5. DOI: 10.1126/science.1132588. Available from: https://www.science.org/doi/abs/10.1126/science.1132588
7. Timmermann A, An SI, Kug JS, Jin Ff, Cai W, Capotondi A, Cobb KM, Lengaigne M, McPhaden MJ, Stuecker MF, Stein K, Wittenberg AT, Yun KS, Bayr T, Chen HC, Chikamoto Y, Dewitte B, Dommenget D, Grothe P, Guilyardi E, Ham YG, Hayashi M, Ineson S, Kang D, Kim S, Kim W, Lee JY, Li T, Luo JJ, McGregor S, Planton Y, Power S, Rashid H, Hongli R, Santoso A, Takahashi K, Todd A, Wang G, Wang G, Ruihuang X, Yang WH, Yeh SW, Yoon J, Zeller E, and Zhang X. El Niño-Southern Oscillation complexity. eng. Nature (London) 2018; 559:535–45
8. Alexander MA and Deser C. A Mechanism for the Recurrence of Wintertime Midlatitude SST Anomalies. eng. Journal of physical oceanography 1995; 25:122–37
9. Holbrook NJ, Scannell HA, Sen Gupta A, Benthuysen JA, Feng M, Oliver ECJ, Alexander LV, Burrows MT, Donat MG, Hobday AJ, Moore PJ, Perkins-Kirkpatrick SE, Smale DA,

Straub SC, and Wernberg T. A global Assessment of Marine Heatwaves and Their Drivers. eng. Nature communications 2019; 10:2624–13

10. Dare RA and McBride JL. Sea Surface Temperature Response to Tropical Cyclones. eng. Monthly weather review 2011; 139:3798–808
11. Jones E, Parfitt R, Wing AA, and Hart R. Gulf Stream Sea Surface Temperature Anomalies Associated With the Extratropical Transition of North Atlantic Tropical Cyclones. eng. Geophysical research letters 2023; 50
12. Zhang Q, Liu B, Li S, and Zhou T. Understanding Models' Global Sea Surface Temperature Bias in Mean State: From CMIP5 to CMIP6. Geophysical Research Letters 2023; 50. e2022GL100888 2022GL100888:e2022GL100888. DOI: https://doi.org/10.1029/2022GL100888. Available from: https://agupubs.onlinelibrary.wiley.com/doi/abs/10.1029/2022GL100888
13. Czaja A and Marshall J. Observations of atmosphere-ocean coupling in the North Atlantic. Quarterly Journal of the Royal Meteorological Society 2001; 127:1893–916. DOI: https://doi.org/10.1002/qj.49712757603
14. Armour KC, Proistosescu C, Dong Y, Hahn LC, Blanchard-Wrigglesworth E, Pauling AG, Jnglin Wills RC, Andrews T, Stuecker MF, Po-Chedley S, Mitevski I, Forster PM, and Gregory JM. Sea-surface temperature pattern effects have slowed global warming and biased warming-based constraints on climate sensitivity. eng. Proceedings of the National Academy of Sciences - PNAS 2024; 121:e2312093121–
15. Peng W, Chen Q, Zhou S, and Huang P. CMIP6 model-based analog forecasting for the seasonal prediction of sea surface temperature in the offshore area of China. eng. Geoscience letters 2021; 8:1–8
16. Wang L, Zhang X, Leung LR, Chiew FHS, AghaKouchak A, Ying K, and Zhang Y. CAS-Canglong: A skillful 3D Transformer model for sub-seasonal to seasonal global sea surface temperature prediction. eng. arXiv.org 2024
17. Dheeshjith S, Subel A, Adcroft A, Busecke J, Fernandez-Granda C, Gupta S, and Zanna L. Samudra: An AI Global Ocean Emulator for Climate. eng. Geophysical research letters 2025; 52
18. Huang B, Liu C, Banzon V, Freeman E, Graham G, Hankins B, Smith T, and Zhang HM. Improvements of the Daily Optimum Interpolation Sea Surface Temperature (DOISST) Version 2.1. Journal of Climate 2021; 34:2923–39. DOI: 10.1175/JCLI-D-20-0166.1. Available from: https://journals.ametsoc.org/view/journals/clim/34/8/JCLI-D-20-0166.1.xml
19. Bulgin CE, Merchant CJ, and Ferreira D. Tendencies, Variability and Persistence of Sea Surface Temperature Anomalies. eng. Scientific reports 2020; 10:7986–
20. Deser C, Alexander MA, and Timlin MS. Understanding the Persistence of Sea Surface Temperature Anomalies in Midlatitudes. Journal of Climate 2003; 16:57–72. DOI: 10.1175/1520-0442(2003)016<0057:UTPOSS>2.0.CO;2. Available from: https://journals.ametsoc.org/view/journals/clim/16/1/1520-0442_2003_016_0057_utposs_2.0.co_2.xml

21. Pickard GL and Emery WJ. Descriptive Physical Oceanography : an Introduction. eng. 5th ed. Oxford: Pergamon, 1990
22. SEANOE, ed. Argo float data and metadata from Global Data Assembly Centre (Argo GDAC). Dataset. 2025. DOI: 10.17882/42182. Available from: https://doi.org/10.17882/42182
23. Wong APS et al. Argo Data 1999–2019: Two Million Temperature-Salinity Profiles and Subsurface Velocity Observations From a Global Array of Profiling Floats. eng. Frontiers in Marine Science 2020; 7
24. Gill AE. Atmosphere-ocean Dynamics. eng. International geophysics series ; v.30. New York ; Academic Press, 1982
25. Cheng L, Abraham J, Hausfather Z, and Trenberth KE. How fast are the oceans warming? Science 2019; 363:128–9. DOI: 10.1126/science.aav7619. Available from: https://www.science.org/doi/abs/10.1126/science.aav7619
26. IPCC, 2023: Sections. In: Climate Change 2023: Synthesis Report. Contribution of Working Groups I, II and III to the Sixth Assessment Report of the Intergovernmental Panel on Climate Change [Core Writing Team, H. Lee and J. Romero (eds.)]. IPCC 2023 :35–115. DOI: 10.59327/IPCC/AR6-9789291691647
27. Fyfe JC, Meehl GA, England MH, Mann ME, Santer BD, Flato GM, Hawkins E, Gillett NP, Xie SP, Kosaka Y, and Swart NC. Making Sense of the Early-2000s Warming Slowdown. eng. Nature climate change 2016; 6:224–8
28. Kerr RA. A North Atlantic climate pacemaker for the centuries. eng. Science (American Association for the Advancement of Science) 2000; 288:1984–6
29. Czaja A. Why Is North Tropical Atlantic SST Variability Stronger in Boreal Spring? Journal of Climate 2004; 17:3017–25. DOI: 10.1175/1520-0442(2004)017<3017:WINTAS>2.0.CO;2. Available from: https://journals.ametsoc.org/view/journals/clim/17/15/1520-0442_2004_017_3017_wintas_2.0.co_2.xml
30. Mantua NJ, Hare SR, Zhang Y, Wallace JM, and Francis RC. A Pacific Interdecadal Climate Oscillation with Impacts on Salmon Production. eng. Bulletin of the American Meteorological Society 1997; 78:1069–79
31. Bond NA, Cronin MF, Freeland H, and Mantua N. Causes and impacts of the 2014 warm anomaly in the NE Pacific. Geophysical Research Letters 2015; 42:3414–20. DOI: https://doi.org/10.1002/2015GL063306
32. Hasselmann K. Stochastic Climate Models: Part I. Theory. Tellus 1976 Jan. DOI: 10.3402/tellusa.v28i6.11316
33. Frankignoul C and Hasselmann K. Stochastic Climate Models: Part II. Application to S-surface Temperature Anomalies and Thermocline Variability. Tellus. 1977 Aug; 29
34. Garwood Jr. RW. A General Model of the Ocean Mixed Layer - Using a Two-Component Turbulent Kinetic Energy Budget with Mean Turbulent Field Closure. NOAA Technical Report ERL 384-PMEL 27 1976 Sep. Available from: https://www.pmel.noaa.gov/pubs/PDF/garw226/garw226.pdf

35. Harcourt RR. An Improved Second-Moment Closure Model of Langmuir Turbulence. Journal of Physical Oceanography 2015; 45:84–103. DOI: 10.1175/JPO-D-14-0046.1. Available from: https://journals.ametsoc.org/view/journals/phoc/45/1/jpo-d-14-0046.1.xml
36. Gaspar P, Grégoris Y, and Lefevre JM. A Simple Eddy Kinetic Energy Model for Simulations of the Oceanic Vertical Mixing: Tests at Station Papa and Long-term Upper Ocean Study Site. Journal of Geophysical Research: Oceans 1990; 95:16179–93. DOI: https://doi.org/10.1029/JC095iC09p16179
37. Burchard H, Craig PD, Gemmrich JR, van Haren H, Mathieu PP, Meier HM, Smith WAMN, Prandke H, Rippeth TP, Skyllingstad ED, Smyth WD, Welsh DJ, and Wijesekera HW. Observational and Numerical Modeling Methods for Quantifying Coastal Ocean Turbulence and Mixing. Progress in Oceanography 2008; 76:399–442. DOI: https://doi.org/10.1016/j.pocean.2007.09.005. Available from: https://www.sciencedirect.com/science/article/pii/S0079661108000050
38. Damerell GM, Heywood KJ, Calvert D, Grant AL, Bell MJ, and Belcher SE. A Comparison of Five Surface Mixed Layer Models with a Year of Observations in the North Atlantic. Progress in Oceanography 2020; 187:102316. DOI: https://doi.org/10.1016/j.pocean.2020.102316. Available from: https://www.sciencedirect.com/science/article/pii/S0079661120300550
39. Large WG, McWilliams JC, and Doney SC. Oceanic Vertical Mixing: A Review and a Model with a Nonlocal Boundary Layer Parameterization. Reviews of Geophysics 1994 Nov; 32:363–403. DOI: https://doi.org/10.1029/94RG01872. Available from: https://agupubs.onlinelibrary.wiley.com/doi/abs/10.1029/94RG01872
40. Price J, Weller R, and Pinkel R. Diurnal Cycling: Observations and Models of the Upper Ocean Response to Diurnal Heating, Cooling, and Wind Mixing. J. Geophys. Res. 1986 Jul; 91:8411–27. DOI: 10.1029/JC091iC07p08411
41. Wallace JM and Hobbs PV. Atmospheric Science : an Introductory Survey. eng. Second edition. International Geophysics Series ; Volume 92. Burlington, Massachusetts: Academic Press, 2006
42. Roemmich D et al. On the Design and Implementation of Argo: an Initial Plan for a Global Array of Profiling Floats. International CLIVAR Project Office Report 21, GODAE Report 5 1998. Available from: https://nla.gov.au/nla.cat-vn2044004
43. Roemmich D and Gilson J. The 2004–2008 Mean and Annual Cycle of Temperature, Salinity, and Steric Height in the Global Ocean from the Argo Program. Progress in Oceanography 2009; 82:81–100. DOI: https://doi.org/10.1016/j.pocean.2009.03.004. Available from: https://www.sciencedirect.com/science/article/pii/S0079661109000160
44. Maze G and Balem K. argopy: A Python library for Argo ocean data analysis. eng. Journal of open source software 2020; 5:2425–
45. Hersbach H, Bell B, Berrisford P, Hirahara S, Horányi A, Muñoz-Sabater J, Nicolas J, Peubey C, Radu R, Schepers D, Simmons A, Soci C, Abdalla S, Abellan X, Balsamo G,

Bechtold P, Biavati G, Bidlot J, Bonavita M, De Chiara G, Dahlgren P, Dee D, Diamantakis M, Dragani R, Flemming J, Forbes R, Fuentes M, Geer A, Haimberger L, Healy S, Hogan RJ, Hólm E, Janisková M, Keeley S, Laloyaux P, Lopez P, Lupu C, Radnoti G, Rosnay P de, Rozum I, Vamborg F, Villaume S, and Thépaut JN. The ERA5 global reanalysis. Quarterly Journal of the Royal Meteorological Society 2020; 146:1999–2049. DOI: https://doi.org/10.1002/qj.3803. Available from: https://rmets.onlinelibrary.wiley.com/doi/abs/10.1002/qj.3803

46. Taburet G, Sanchez-Roman A, Ballarotta M, Pujol MI, Legeais JF, Fournier F, Faugere Y, and Dibarboure G. DUACS DT2018: 25 years of reprocessed sea level altimetry products. Ocean Science 2019; 15:1207–24. DOI: 10.5194/os-15-1207-2019. Available from: https://os.copernicus.org/articles/15/1207/2019/

47. Large WG and Pond S. Sensible and Latent Heat Flux Measurements over the Ocean. Journal of Physical Oceanography 1982; 12:464–82. DOI: 10.1175/1520-0485(1982)012<0464:SALHFM>2.0.CO;2. Available from: https://journals.ametsoc.org/view/journals/phoc/12/5/1520-0485_1982_012_0464_salhfm_2_0_co_2.xml

48. Seo H, O'Neill LW, Bourassa MA, Czaja A, Drushka K, Edson JB, Fox-Kemper B, Frenger I, Gille ST, Kirtman BP, Minobe S, Pendergrass AG, Renault L, Roberts MJ, Schneider N, Small RJ, Stoffelen A, and Wang Q. Ocean Mesoscale and Frontal-Scale Ocean–Atmosphere Interactions and Influence on Large-Scale Climate: A Review. eng. Journal of climate 2023; 36:1981–2013